JES Focus Issue on Processes at the Semiconductor-Solution Interface

Water Interaction with Sputter-Deposited Nickel Oxide on n-Si Photoanode: Cryo Photoelectron Spectroscopy on Adsorbed Water in the Frozen Electrolyte Approach

Mathias Fingerle,[z] Sven Tengeler, Wolfram Calvet, Thomas Mayer, and Wolfram Jaegermann

Surface Science Division, Department of Materials Science, Technical University Darmstadt, D-64287 Darmstadt, Germany

The interaction of water with a magnetron-sputtered nickel oxide thin film on an n-type silicon photoanode is investigated in perspective to oxygen evolution. The substrate was exposed in-situ stepwise to gas phase water up to 10 L at liquid N_2 temperature and analyzed via X-ray and UV photoelectron spectroscopy in the so called frozen electrolyte approach. Photoemission of the pristine NiO_x layer shows the presence of stoichiometric NiO and Ni_2O_3 as well as of non-stoichiometric phases. In the monolayer range, molecular and dissociative adsorption is detected assigned to the NiO respective Ni_2O_3 phase. Initially, the emission of the molecular adsorbed water species interacting with NiO is found at 0.8 eV lower binding energies as compared to water related emission for higher coverages with binding energies commonly assigned to H_2O-H_2O interaction. In addition to the chemical analysis, the electronic structure of the n-Si/SiO_x/NiO_x/H_2O photoanode is measured and discussed.
 [DOI: 10.1149/2.0191804jes]

Manuscript submitted October 23, 2017; revised manuscript received December 21, 2017. Published February 2, 2018. *This paper is part of the JES Focus Issue on Processes at the Semiconductor-Solution Interface.*

Most semiconducting materials, especially silicon, are unstable and degrade or passivate rapidly under photoanodic conditions in aqueous electrolytes.[1] Nickel oxide thin films are promising catalysts for the hydrogen and the oxygen evolution reaction (OER)[2] and provide chemically stable coatings for silicon, while being transparent, antireflective and electronically conductive in addition.[3–5] Elementary charge transfer processes located at a solid/liquid interface, are still scarcely approached by scientific studies on an atomistic scale.[6] Especially the energetics of the photocatalytic dissociation of water on semiconducting materials is still unclear. In general, the determination of the chemical and electronic interaction at the interface between metal oxides and liquid electrolytes on an atomistic scale via surface science methods suffers from the so-called pressure gap.[7,8] One way to bridge the gap, model experiments at low temperatures can be utilized to monitor the surface chemistry by means of photoelectron spectroscopy under ultra-high vacuum. Regarding double layer formation, the frozen-electrolyte approach has already shown its potential in the past.[9]

The principle mechanism of the oxygen evolution (OER) at nickel hydroxide based electrodes was investigated early on a more chemical basis[10] with various phase transitions involved.[11] It has been found that $Ni(OH)_2$ and NiOOH species at the surface are a prerequisite for any photocatalytic activity. However, the exact mechanism is still under debate[12] with the role of nickel oxide only little discussed. A first step for a better understanding is to study the reactivity of a pristine nickel oxide surface upon water adsorption. For NiO(100) it has been demonstrated that a perfect surface exhibits no reactive interaction with H_2O unless oxygen vacancies induce the dissociation of water[13] or adsorbed O^{2-} ions at defect sites on a pre-oxidized surface enhance the reactivity. In contrast to NiO(100), theoretical studies predict dissociative water adsorption for NiO(111).[14] Further to oxygen vacancies sub-coordinated Ni surface atoms are active in dissociative water adsorption.[15] It also has been found that Ni increases the OER activity of iron oxide and vice versa.[16] Thereby, the photocatalytic performance of hematite can be dramatically enhanced by the formation of a hematite-NiO/α-$Ni(OH)_2$ composite heterostructure.[17] However, no literature was found for Ni_2O_3 as an effective catalyst for water splitting. Obviously, there are many open questions dealing with the interaction of water with nickel oxide on an atomic scale revealing the exact reaction paths and the according energy schemes. In this publication we present in-situ X-ray (XPS) and UV-photoelectron spectroscopy (UPS) analysis of stepwise adsorbed water on a magnetron-sputtered thin NiO film grown on thermally oxidized n-doped silicon. During the interface experiment under dark condition, the sample was kept at LN temperature in order to suppress instantaneous desorption of water in this cryogenic photoelectron spectroscopy (CryoPES) approach.

Experimental

Sample preparation.—A 4-inch (001) phosphor doped n-type silicon wafer was cleaned in an ultrasonic bath for 10 min. in acetone, isopropanol and ultra-pure water each. In order to produce a hydrogen terminated surface, it was then etched in H_2SO_4:H_2O_2 = 2:1 at 80°C for 10 min., rinsed with ultra-pure water, followed by a 10 min. oxide removal step in 5% HF. Afterwards it was rinsed with ultra-pure water, etched again in in H_2SO_4:H_2O_2 = 2:1 at 80°C for 10 min., rinsed, and subjected to a second 6 min. oxide removal step in NH_4F.[18] Chemicals used (all VLSI standards) were 96% H_2SO_4, 31% H_2O_2, 5% HF, and 40% NH_4F. The sample was then thoroughly rinsed and dried under nitrogen flow, before being introduced into the ultra-high vacuum (UHV) deposition and analysis system Darmstadt Integrated System for Fundamental Research (DAISY-Fun)[19] within 5 min.

Following the growth of an 8 Å thermal oxide layer, NiO_x was deposited on the sample via reactive magnetron sputtering. The NiO_x deposition was performed in-situ in a deposition chamber with a base pressure of $8 \cdot 10^{-8}$ mbar, under 19.6 sccm Ar (99.999% pure) and 0.4 sccm O_2 (99.995% pure) flow at 0.03 mbar, using a 99.99% pure nickel target at 15 W. A total deposition time of 540 s resulted in a 39 Å NiO_x layer as determined from the relative intensities of the Ni 2p and Si 2p XPS core level spectra.[20]

Interface experimental.—Ultra-pure water was filled into a Schlenk-type glass flask connected to a separated adsorption chamber with a base pressure of $1 \cdot 10^{-9}$ mbar. Freeze-pump cycling was used to purify the water. The dosage was controlled by a leak valve and the exposure time was varied stepwise to match the desired dosage from 0.1 L (Langmuir) to 10 L using uncorrected pressure readings. The sample was transferred on a LN-cooled manipulator from the adsorption chamber to the analysis chamber both held at a base pressure of $5 \cdot 10^{-10}$ mbar for consecutive photoelectron spectroscopy. The sample was not subject to light irradiation to avoid unwanted photocatalytic reactions during the experiment. The analysis chamber

[z]E-mail: mfingerle@surface.tu-darmstadt.de

Table I. Full width at half maximum (FWHM) and initial binding energies in eV for the Ni2p$_{3/2}$ and O1s core level components derived from XPS measurements.

Core level	Component	FWHM [eV]	Binding energy [eV]
Ni2p$_{3/2}$	Peak I	1.1	854.0
	Peak II	3.2	855.7
	sat I	3.7	860.8
	sat II	4.7	864.0
O1s	NiO	1.0	529.8
	NiOOH	1.0	530.6
	$Ni(OH)_2$	1.0	531.1
	Ni_2O_3	1.65	531.2
	NiOOH	1.0	532.2
	H_2O-NiO	1.3	532.7
	SiO_x	1.4	533.0
	H_2O-H_2O	1.5	533.5

is equipped with a SPECS Phoibos 150 analyzer and a SPECS Focus 500 X-ray source using the monochromatized AlK$_\alpha$ line at 1486.74 eV for XPS and the HeI (21.2 eV) and HeII (40.8 eV) lines for UPS. In order to determine the workfunction, a bias-voltage of −3 V was applied. The interface experiment started with the analysis of the pristine nickel oxide surface, followed by four deposition steps of frozen water leading to a thickness of 0.1 L, 0.4 L, 1.6 L, and 10 L. At the end, the sample was slowly heated up to room temperature (RT) and measured again.

Spectra analysis.—The XP spectra were background subtracted using the Shirley method,[21] while for the UP spectra a Tougaard background was subtracted.[22] All UP spectra were HeI- and HeII-satellite corrected, respectively. A sputtered Au foil served as reference sample in order to calibrate the spectrometer by making use of the Au4f$_{7/2}$ transition at 84.0 eV. The XPS core level peaks were fitted using a pseudo-Voigt function with a fixed ratio of 0.2 between the Lorentzian and Gaussian distributions. As a result, binding energy, line width and intensity are obtained and compared on a qualitative basis. Beyond that, intensity changes within the same region (e.g. O1s or Ni2p) were treated on a quantitative basis since cross section and kinetic energy are unchanged. The full width at half maximum (FWHM) and the initial binding energies for the deconvolution of the Ni2p$_{3/2}$ and O1s core level are given in Table I. The parameters for the Ni2p$_{3/2}$ components were chosen based on literature.[23] The FWHM of the NiO component in the O1s core level was calculated by peak fitting of the pristine spectrum. The FWHM and binding energy of the SiO_x component was deduced from the n-Si/SiO_x spectrum previous to nickel oxide deposition. The larger values for the FWHM of the Ni_2O_3, H_2O-NiO and H_2O-H_2O component are caused by the structurally less defined nature of these phases and the exact numerical values were optimized by the fitting routine. Additional information is provided in the discussion.

Results and Discussion

Surface chemistry.—In contrast to the complex and controversially discussed nature of the Ni2p core level emission,[24–27] the nickel oxide substrate, hydroxylated species and molecular water can be discriminated clearly in the O1s core level. Additionally, the O1s peak provides information of the full NiO thin film, as it has a thickness of less than 5 nm and the SiO_2 peak of the underlying silicon is still detectable for the pristine substrate as shown in Figure 1a. The main feature at 529.4 eV is assigned to the O^{2-} lattice oxygen.[23,28] For the pristine layer the broader structure at higher binding energies is assigned to Ni_2O_3, but upon water exposure also hydroxylated nickel oxide species appear in this binding energy region.[23,28] Initially, a strongly attenuated silicon oxide peak and minor carbon oxide contaminations are present around 533.0 eV.

With increasing water adsorption, the broader structure at higher binding energies changes and can only be satisfyingly reproduced,

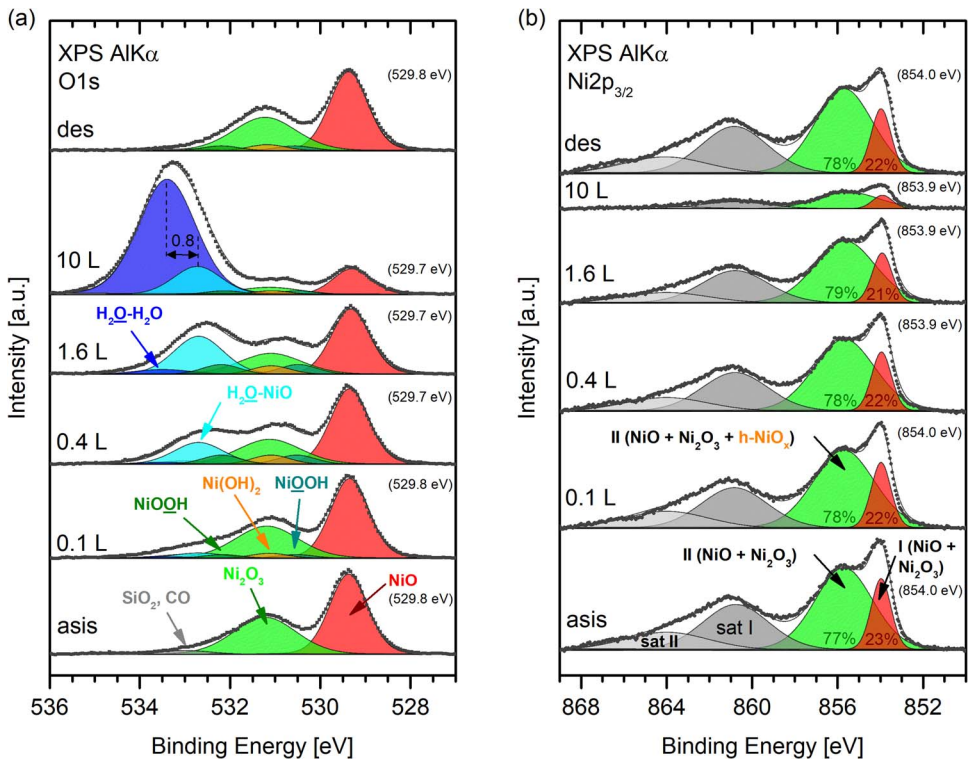

Figure 1. XPS AlK$_\alpha$ O1s (a) and Ni2p$_{3/2}$ (b) core level of the stepwise water adsorption and desorption on n-Si/SiO_x/NiO_x. Indicated are the contributions of the peak fit and the binding energy of the peak maximum. The hydroxylated nickel oxide species NiOOH and $Ni(OH)_2$ are summarized as h-NiO_x in (b). For simplicity, the Ni spectra are fitted with Voight functions to the main emissions of NiO and Ni_2O_3 ignoring shoulders that lead to an overlap.

when taking three different hydroxide species into account. Considering partial charge in the initial state the components at 530.6 eV, 531.2 eV, and 532.2 eV can be assigned to NiOOH, $Ni(OH)_2$ and NiOOH species, respectively. The species to which the respective oxygen emission is assigned is indicated by an underline in the molecule formula. Nickel oxide hydroxide species are known to be present as surface layer on nickel oxide in contact with water or aqueous electrolytes.[23,28,29] The different hydroxides can be reliably distinguished according to recent combined XPS and IR studies.[30]

With increasing water exposure, a new feature arises at around 533.0 eV that can be fitted satisfyingly with two components at 532.7 eV and 533.5 eV, respectively. The latter one is typical for interacting H_2O molecules in a multilayer film.[31–35] However, up to a water exposure of 1.6 L, the species at 532.7 eV is dominant and only for 10 L, the species at 533.5 eV becomes predominant. As in the UP spectra below the fingerprint of molecular water is observed at low water exposure, we assign the first species at 532.7 eV to a H_2O-NiO surface species, physisorbed onto stoichiometric nickel oxide.

Remarkably, the signal of stoichiometric NiO is only affected by the general attenuation due to the water adsorption, while the initial Ni_2O_3 emission changes its line shape due to additional components of hydroxylated species. After annealing to room temperature, these hydroxylated species partly remain on the surface. From a more accurate peak fitting of the O1s core level, we deduce that mainly Ni_2O_3 and presumably defect sites including phase boundaries are reactive upon water adsorption while on NiO water is physisorbed. This corresponds to experiments on NiO(100) single crystals which show no dissociative water adsorption.[13] In general, the reactivity of nickel oxide toward water depends on crystal orientation,[13,14] pretreatment,[13,36] and Ni sub-coordination at the surface.[15] As the NiO phase is not exclusively (100) terminated it will add to a small extent also to dissociative water adsorption.

The evolution of the $Ni2p_{3/2}$ core level for the stepwise water adsorption and desorption is shown in Figure 1b. The nature of the Ni2p structure is complex, dominated by correlation effects of the valence band, including multiplet structures[24,25] and final state effects.[26,27] Using a four component fit, the Ni2p emission can be well approximated.[23] For the pristine sample the emissions of Ni^{2+} in NiO[23,28] and Ni^{3+} in Ni_2O_3[29,37–39] as well as non-stoichiometric phases have overlapping shoulders that contribute to the simple Voigt peaks I at 854.0 eV and II at 855.7 eV. Additionally, the broader feature at 855.7 eV is known to include contributions from hydroxylated species, namely $Ni(OH)_2$ (Ni^{2+})[24,28,29,37] and NiOOH (Ni^{3+})[15,24,40] that are all summarized under the term h-NiO_x. Unfortunately, further stoichiometric phases cannot be deconvoluted here due to their complex signature.[23,28] Despite of the ambiguity of the Ni2p core level emissions, the relative changes of peak II compared to peak I supply information about the formation of surface hydroxides.

The satellite region of the Ni2p core level consists of two broad features at 860.8 eV (sat I) and 864 eV (sat II), which are affected in intensity by the transformation of nickel oxide to hydroxylated species as well as by the transformation of $Ni(OH)_2$ to NiOOH.[24,40] Due to the water-free preparation under UHV conditions emissions from hydroxylated nickel species can be excluded in the Ni2p spectrum of the pristine nickel oxide thin film (asis). Upon stepwise water adsorption, the relative peak area of peak II compared to peak I rises from 77 to 79% as denoted in Figure 1b. After desorption, this value decreases marginally to 78%. In compliance to the observations of the O1s core level, the relative increase of peak II indicates the formation of h-NiO_x species at the surface that remain on the surface after desorption.

In the valence band region of nickel oxide, molecular water and dissociated water species are known for unique fingerprints.[13,41] In Figure 2, consecutive HeII valence band spectra upon water adsorption and after desorption are correlated to respective difference spectra in which the emission of the pristine sample has been eliminated. All spectra are satellite corrected and normalized to the Ni3d peak maximum. Weak peak structures at 4.6 eV and 7.9 eV in the difference spectra are attributed to the 1π and 1σ orbitals of OH^- from

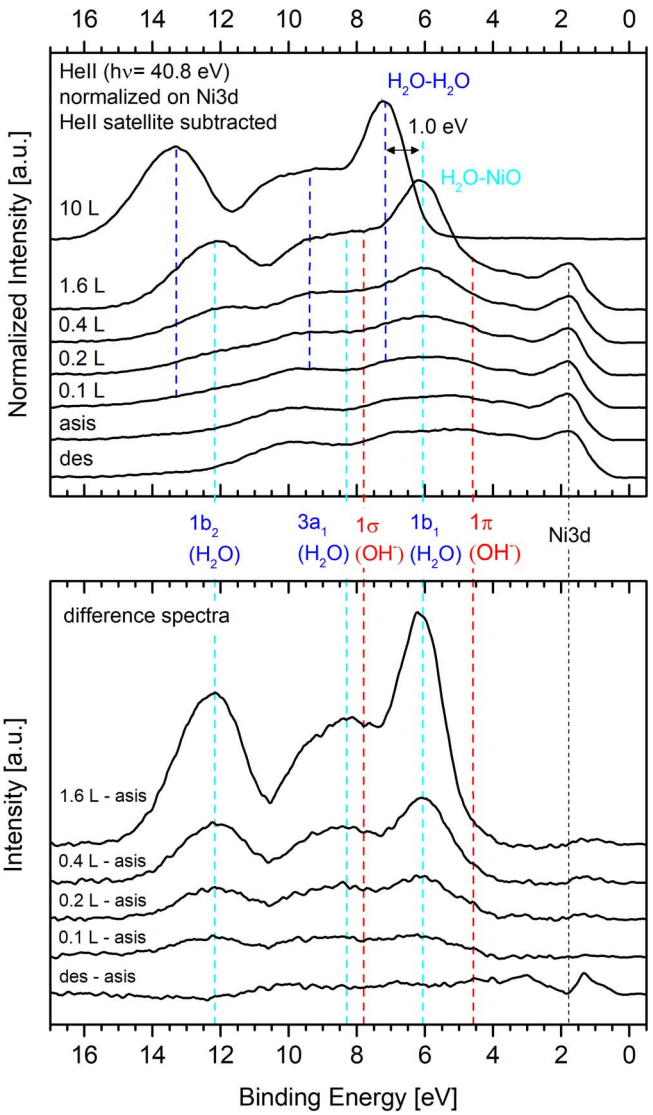

Figure 2. Valence band spectra recorded with HeII for stepwise water adsorption and after desorption normalized to the Ni3d emission (top). In the according difference spectra, the spectrum of the pristine sample is subtracted (bottom). Binding energies of molecularly adsorbed H_2O and OH^- species are assigned, respectively. In addition, the binding energy distance between the two different molecular water species, H_2O-NiO and H_2O-H_2O is highlighted.

dissociative water adsorption.[31,42] The binding energy distance between the two peaks is about 3.3 eV. On NiO(100)[13] a similar separation in the binding energy of 3.3 eV has been reported for OH^-. Presumably, the exact energy distance is depending on the reaction mechanism, oxidation state and adsorption site. The features are most intense after 0.1 L water adsorption and are still observable after desorption indicating water dissociation due to the nickel oxide surface and in part chemisorption of OH^-. By taking the XPS results into account, the OH valence band features can be assigned to the formation of $Ni(OH)_2$ and NiOOH in the surface region. Moreover, the unique fingerprint of molecularly adsorbed water is clearly visible in the difference spectra after 0.1 L. But the distinct features at 6.1 eV ($1b_1$ orbital), 12.1 eV ($1b_2$ orbital), and around 8.4 eV ($3a_1$ orbital) are usually expected at about 1 eV higher binding energies[31,42] in case of hydrogen bond and dipole-dipole interacting water molecules in a multilayer. We relate the water emissions at lower binding energy to water molecules physisorbed to nonreactive NiO surfaces. After 10 L water adsorption the water emission shifts to higher binding energies typical for multilayer water. Due to the supreme surface sensitivity

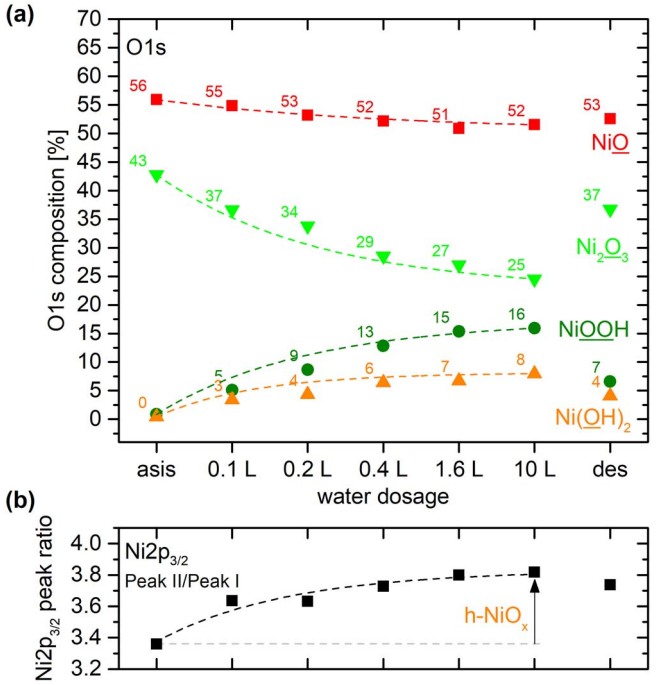

Figure 3. Composition of the nickel oxide thin film surface deduced from different O1s core level peak components (a) and ratio of peak II (NiO + Ni_2O_3 + h-NiO_x) to peak I (NiO + Ni_2O_3) deduced from the $Ni2p_{3/2}$ peak fit (b) during stepwise water adsorption and desorption. The hydroxylated nickel oxide species NiOOH and $Ni(OH)_2$ are summarized as h-NiO_x in (b).

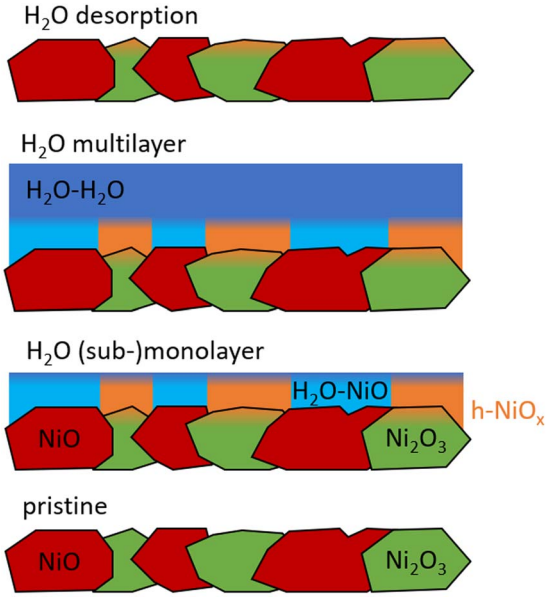

Figure 4. Schematic model of the interface formation between a sputtered nickel oxide thin film and adsorbed water. Hydroxylated nickel oxide species are denoted as h-NiO_x.

using HeII excitation, only emissions from bulk water species and no substrate emissions are visible after 10 L exposure. With increasing water dosage, the emissions from Ni3d states shape a shoulder toward lower binding energies that appears as small peak in the difference spectra with a maximum at around 1.2 eV of increasing intensity. This emission is attributed to Ni3d interface states related to the water dissociation process. To obtain the least structured difference spectrum after desorption in the water emission region, the Ni3d peaks were shifted slightly against each other leading to the zick-zack structure.

Figure 3a visualizes chemical processes based on an evaluation of the percental peak areas of the components in the O1s spectra excluding the molecular water species. By this approach, the general attenuation of the signal is ruled out. With increasing water dosage, the NiO concentration is slightly decreasing which indicates some minor reactivity only. In contrast, the Ni_2O_3 concentration shows a distinct decrease and therefore enhanced reactivity while the presence of $Ni(OH)_2$ and NiOOH gradually increases. After desorption, this process is not fully reversed leaving traces of $Ni(OH)_2$ and NiOOH on the surface. This is in agreement to the HeII valence band spectra where OH^- residuals can be detected in the difference spectra after desorption as well. We conclude, while some chemisorbed OH^- species remain on the surface after desorption, most of the h-NiO_x species vanish from it. Presumably, the respective OH groups are reversibly bonded at RT while they get solvated. For practical use, this could be beneficial since possible reactive sites at the surface will not be passivated irreversibly.

In the Ni2p core level, the variety of complex species cannot be fully resolved. Nevertheless, the Ni2p core level is slightly more surface sensitive than the O1s core level which gives at least a further indication. In addition to Figure 1a, the ratio between peak II and peak I is plotted as function of water exposure. Since hydroxylated nickel species h-NiO_x are only present in peak II, an increase is most likely corresponding to the formation of NiOOH and $Ni(OH)_2$. And indeed, the ratio is slightly increasing upon water adsorption, from 3.4 for the pristine nickel oxide thin film to 3.8 after exposure to 10 L. After desorption, the ratio only slightly decreases again to 3.7. This gives further rise to the assumption that mainly the Ni atoms act as docking sites for hydroxylated nickel species h-NiO_x. In total, the results from XPS core level and UPS valence band analysis draw a consistent and plausible picture of the surface chemistry upon water adsorption which allows us to create a schematic interface model.

Adapted from our photoemission data the surface chemistry is discussed on the basis of a simple model that represents different phases and possible phase boundaries as drawn in the schematic in Figure 4. Due to the critical thickness of only a few nanometers, we were not able to obtain quantitative structural information about the nickel oxide thin film in the course of this study. However, the pristine magnetron-sputtered nickel oxide thin film presumably consists of small nano-crystallites that represent different phases of nickel oxide: NiO with an oxidation state of Ni^{2+} and Ni_2O_3 with a formal oxidation state of Ni^{3+}. Additional defect sites have to be considered that may play a crucial role for the reactivity of the surface.[13,43] Recent in operando NEXAFS and EIS studies on iron oxide underline the importance of oxygen defect states for the formation of hydroxyl groups at metal oxide surfaces as a preliminary stage of water-splitting.[44] Indeed, XPS analysis indicates that upon water adsorption, predominantly the Ni_2O_3 phase and presumably defective sites and phase boundaries are reactive. If water dissociates, hydroxylated species form (h-NiO_x). In contrast, water mostly physisorbs on NiO (H_2O-NiO) which leads to the observation of the molecular water surface species with emissions at around 1 eV lower binding energies as compared to the multilayer regime when the typical H_2O-H_2O interaction is dominant. After desorption, the two molecular water species are fully removed from the surface. Only some chemisorbed hydroxylated h-NiO_x species remain. As already mentioned, besides the stoichiometric phase, multiple surface characteristics are known to influence water dissociation: Crystal orientation, defect sites, bond saturation and pretreatment with oxygen plasma amongst others. Especially the fact, that Ni_2O_3 shows a much higher reactivity compared to NiO should be further pursued with regard to an application as OER catalyst.

Energy level alignment.—Figure 5a schematically shows the band diagram of the layered n-Si/SiO_x/NiO_x system before and after water adsorption. The thickness of the intermediate SiO_x layer is about 2–3 nm. The band bending upward of the n-Si toward the oxide layer was calculated to be 0.4 eV considering the bulk position of the valence

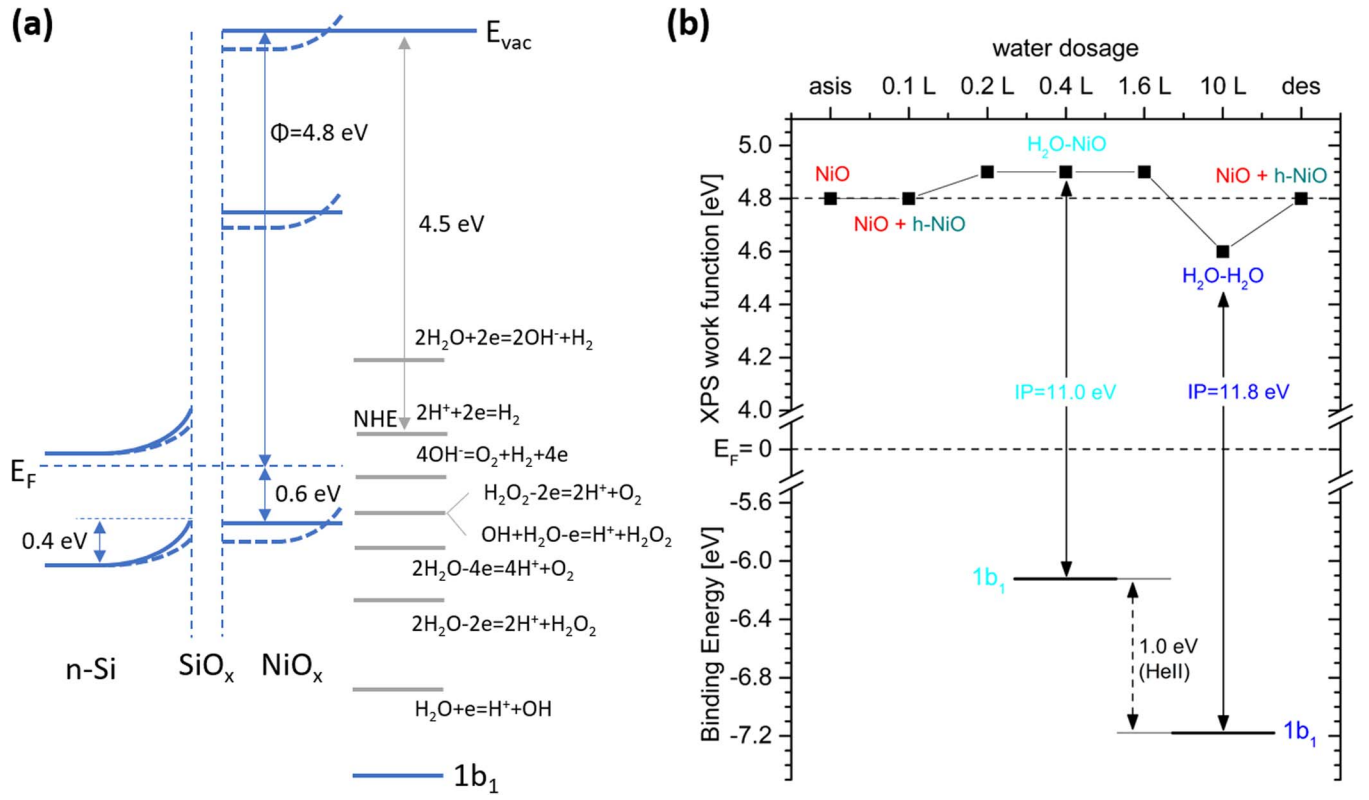

Figure 5. Energy level alignment for water adsorption on a nickel oxide thin film magnetron sputtered on n-Si/SiO_x in relation to redox potentials of the H_2O catalysis (a). Evolution of the work function of the sample complemented by some ionization potentials IP of the $1b_1$-orbital of H_2O-NiO and H_2O-H_2O molecular water species (b). The reversible band bending upon water adsorption is indicated in (a) as dashed lines. The bandgap of the NiO_x thin film has been given based on literature.[46]

band maximum according to doping concentration and the measured position. The sputtered nickel oxide thin film has a thickness of less than 5 nm. The valence band maximum is measured about 0.6 eV below the Fermi-level and the work function was calculated from the secondary electron onset (not shown in the spectra) to be Φ_{NiO} = 4.8 eV. Both values correspond well to identically prepared thin films[45] as well as to solution processed NiO_x films.[28] For the bandgap of the NiO_x thin film a value of 3.7 eV has been assumed based on literature.[46] Upon water adsorption, gradual energy level shifts were detected in the range of 100 meV. However, while the Si2p core level shifts 0.1 eV to lower binding energies, the nickel oxide core level shift 0.1 eV to higher binding energies. This means that the water induced band bending at the NiO_x/H_2O interface is about 0.2 eV. The energy level positions and band bending of the n-Si/SiO_x/NiO_x photoanode in contact with water is indicated as dashed lines in Figure 5a. After water desorption the band bending is nearly fully reversed.

The energy band diagram, charge transfer processes and catalytic activity of an n-Si/NiO_x photoanode without an SiO_x interlayer are discussed in Ref. 3. In the present case, the band bending upwards promotes the migration of photo-generated holes into the NiO_x thin film during water splitting. But in contrast to the n-Si/NiO_x interface discussed in Ref. 3, the SiO_x interlayer reduces the valence band offset between n-Si and NiO_x significantly, facilitating hole transfer. On the other hand, the insufficient charge transport in SiO_x might have a negative influence on the general performance. At the NiO_x/H_2O interface, a slight band bending upwards supports hole transport toward the electrolyte. For practical use, the NiO_x surface is usually electrochemically activated and transforms into a h-NiO_x layer.[47–49] In the present model experiment, we observe the formation of an h-NiO_x layer upon contact to water even without activation. Therefore, by engineering the NiO_x surface, the catalytic performance could be further enhanced. Strategies to increase the fraction of Ni_2O_3 phases and possibly induce defect sites could be post-annealing or oxygen plasma treatment, amongst others. Although the work function is always a parameter of the whole sample, the evolution shown in Figure 5b demonstrates that the work function changes upon water adsorption are mainly governed by the dominant water species in the (sub-) monolayer and multilayer regime, respectively. Between 0.2 L and 1.6 L, where H_2O-NiO species are dominant, the work function is slightly increasing from 4.8 eV for pristine NiO_x to 4.9 eV. Only for water coverages in the multilayer regime, where H_2O-H_2O interaction becomes dominant, the work function is decreasing by 0.3 eV to 4.6 eV. After desorption, the work function increases again to 4.8 eV. With photoemission only one integrated work function value for a polymorphous film can be measured. Using these integrated work function values, the ionization potential IP of the $1b_1$ orbital is considerably higher for the H_2O-H_2O species (IP = 11.8 eV) than for the H_2O-NiO species (IP = 11.0 eV). This might be an important fact for water-splitting but local work function variations have to be considered in addition.

Conclusions

Magnetron-sputtered nickel oxide thin films on thermally oxidized n-type silicon were prepared. Stoichiometric NiO and Ni_2O_3 phases were found but non-stoichiometric portions and defects have to be considered in addition. Upon water adsorption, dissociative water was predominantly observed on Ni_2O_3 including respective defect sites and phase boundaries. Furthermore, the formation of $Ni(OH)_2$ and NiOOH was proven with UPS and XPS. Two different molecularly adsorbed water species could be distinguished: In the (sub-) monolayer regime, the interaction of H_2O with inert NiO over hydrogen bonds was dominant (H_2O-NiO) while in the multilayer regime a second species was detected which shows the typical binding energies of multilayer water. After water desorption induced by heating up to RT, only traces of chemisorbed $Ni(OH)_2$ and NiOOH species were left on the surface. In principal, the band diagram of the

n-Si/SiO_x/NiO_x photoanode in contact to water exhibits a beneficial alignment for the hole transport to the electrode/electrolyte interface. Additionally, the difference in binding energy of the observed water species (H_2O-NiO versus H_2O-H_2O) points to a high usability of nickel oxide and its derivatives with respect to photocatalysis. The experiments demonstrate that surface sensitive information on the reactivity of the solid/liquid interface can be obtained under highly controlled conditions in the UHV on an atomic scale by CryoPES.

Acknowledgments

The manuscript was written through contributions of all authors. They all have given approval to the final version of the manuscript. Financial support through the project "fundamentals of electro-chemical phase boundaries at semiconductor/electrolyte interfaces" GEP-HE funded by the German Federal Ministry of Education and Research BMBF under contract 13XP5023A and by the European Union under the a-leaf project (732840-A-LEAF) is gratefully acknowledged.

References

1. S. Haussener, C. Xiang, J. M. Spurgeon, S. Ardo, N. S. Lewis, and A. Z. Weber, "Modeling, simulation, and design criteria for photoelectrochemical water-splitting systems," *Energ Environ Sci*, **5**, 9922 (2012).
2. D. A. Corrigan and R. M. Bendert, "Effect of Coprecipitated Metal Ions on the Electrochemistry of Nickel Hydroxide Thin Films: Cyclic Voltammetry in 1M KOH" *J Electrochem Soc*, **136**, 723 (1989).
3. L. He, W. Zhou, D. Cai, S. S. Mao, K. Sun, and S. Shen, "Pulsed laser-deposited n-Si/NiOx photoanodes for stable and efficient photoelectrochemical water splitting," *Catalysis Science & Technology*, **7**, 2632 (2017).
4. B. Mei, A. A. Permyakova, R. Frydendal, D. Bae, T. Pedersen, P. Malacrida, O. Hansen, I. E. Stephens, P. C. Vesborg, and B. Seger, "Iron-treated NiO as a highly transparent p-type protection layer for efficient Si-based photoanodes," *The journal of physical chemistry letters*, **5**, 3456 (2014).
5. K. Sun, M. T. McDowell, A. C. Nielander, S. Hu, M. R. Shaner, F. Yang, B. S. Brunschwig, and N. S. Lewis, "Stable solar-driven water oxidation to O_2 (g) by Ni-oxide-coated silicon photoanodes," *The journal of physical chemistry letters*, **6**, 592 (2015).
6. T. Mayer, K. Schwanitz, B. Kaiser, A. Hajduk, M. V. Lebedev, and W. Jaegermann, "Semiconductor/electrolyte interfaces for solar energy conversion: interface studies by synchrotron induced photoelectron spectroscopy," *J Electron Spectrosc*, DOI (2017).
7. H. Bluhm, "Photoelectron spectroscopy of surfaces under humid conditions," *J Electron Spectrosc*, **177**, 71 (2010).
8. E. J. Crumlin, Z. Liu, H. Bluhm, W. Yang, J. Guo, and Z. Hussain, "X-ray spectroscopy of energy materials under in situ/operando conditions," *J Electron Spectrosc*, **200**, 264 (2015).
9. T. Mayer, M. V. Lebedev, R. Hunger, and W. Jaegermann, "Synchrotron photoemission analysis of semiconductor/electrolyte interfaces by the frozen-electrolyte approach: interaction of HCl in 2-propanol with GaAs (100)," *The Journal of Physical Chemistry B*, **110**, 2293 (2006).
10. P. Oliva, J. Leonardi, J. Laurent, C. Delmas, J. Braconnier, M. Figlarz, F. Fievet, and A. De Guibert, "Review of the structure and the electrochemistry of nickel hydroxides and oxy-hydroxides," *J Power Sources*, **8**, 229 (1982).
11. H. Bode, K. Dehmelt, and J. Witte, "Zur kenntnis der nickelhydroxidelektrode—I. Über das nickel (II)-hydroxidhydrat," *Electrochimica Acta*, **11**, 1079IN1071 (1966).
12. O. Diaz-Morales, D. Ferrus-Suspedra, and M. T. M. Koper, "The importance of nickel oxyhydroxide deprotonation on its activity toward electrochemical water oxidation," *Chemical Science*, **7**, 2639 (2016).
13. J. M. McKay and V. E. Henrich, "Surface electronic structure of NiO: defect states, O 2 and H 2 O interactions," *Phys Rev B*, **32**, 6764 (1985).
14. W. Zhao, M. Bajdich, S. Carey, A. Vojvodic, J. K. Nørskov, and C. T. Campbell, "Water Dissociative Adsorption on NiO(111): Energetics and Structure of the Hydroxylated Surface," *ACS Catalysis*, **6**, 7377 (2016).
15. A. G. Marrani, V. Novelli, S. Sheehan, D. P. Dowling, and D. Dini, "Probing the redox states at the surface of electroactive nanoporous NiO thin films," *Acs Appl Mater Inter*, **6**, 143 (2013).
16. M. W. Louie and A. T. Bell, "An Investigation of Thin-Film Ni-Fe Oxide Catalysts for the Electrochemical Evolution of Oxygen," *J. Am. Chem. Soc.*, **135**, 12329 (2013).
17. D. K. Bora, A. Braun, R. Erni, U. Muller, M. Dobeli, and E. C. Constable, "Hematite-NiO/small alpha]-Ni(OH)2 heterostructure photoanodes with high electrocatalytic current density and charge storage capacity," *Phys Chem Chem Phys*, **15**, 12648 (2013).
18. W. Kern, "The evolution of silicon wafer cleaning technology," *J Electrochem Soc*, **137**, 1887 (1990).
19. W. Jaegermann, B. Kaiser, J. Ziegler, and J. Klett, "Interface Engineering of Semiconductor Electrodes for Photoelectrochemical Water Splitting: Application of Surface Characterization with Photoelectron Spectroscopy," Photoelectrochemical Solar Fuel Production, Springer, pp. 199 2016.
20. M. Seah and S. Spencer, "Ultrathin SiO2 on Si II. Issues in quantification of the oxide thickness," *Surf Interface Anal*, **33**, 640 (2002).
21. D. A. Shirley, "High-Resolution X-Ray Photoemission Spectrum of Valence Bands of Gold," *Phys Rev B*, **5**, 4709 (1972).
22. S. Tougaard, "Quantitative analysis of the inelastic background in surface electron spectroscopy," *Surf Interface Anal*, **11**, 453 (1988).
23. M. A. Peck and M. A. Langell, "Comparison of nanoscaled and bulk NiO structural and environmental characteristics by XRD, XAFS, and XPS," *Chem Mater*, **24**, 4483 (2012).
24. A. P. Grosvenor, M. C. Biesinger, R. S. C. Smart, and N. S. McIntyre, "New interpretations of XPS spectra of nickel metal and oxides," *Surf Sci*, **600**, 1771 (2006).
25. R. Gupta and S. Sen, "Calculation of multiplet structure of core p-vacancy levels. II," *Phys Rev B*, **12**, 15 (1975).
26. M. Taguchi, M. Matsunami, Y. Ishida, R. Eguchi, A. Chainani, Y. Takata, M. Yabashi, K. Tamasaku, Y. Nishino, and T. Ishikawa, "Revisiting the valence-band and core-level photoemission spectra of NiO," *Phys Rev Lett*, **100**, 206401 (2008).
27. F. U. Hillebrecht, J. C. Fuggle, P. A. Bennett, Z. Zołnierek, and C. Freiburg, "Electronic structure of Ni and Pd alloys. II. X-ray photoelectron core-level spectra," *Phys Rev B*, **27**, 2179 (1983).
28. E. L. Ratcliff, J. Meyer, K. X. Steirer, A. Garcia, J. J. Berry, D. S. Ginley, D. C. Olson, A. Kahn, and N. R. Armstrong, "Evidence for near-surface NiOOH species in solution-processed NiO x selective interlayer materials: impact on energetics and the performance of polymer bulk heterojunction photovoltaics," *Chem Mater*, **23**, 4988 (2011).
29. K. Kim and N. Winograd, "X-ray photoelectron spectroscopic studies of nickel-oxygen surfaces using oxygen and argon ion-bombardment," *Surf Sci*, **43**, 625 (1974).
30. F. Ullrich, S. Hillebrandt, S. Hietzschold, V. Rohnacher, W. Jaegermann, A. Pucci, W. Kowalsky, R. Lovrincic, S. -b. Beck, and E. Mankel, Annealing temperature dependent analytical study on oxygen plasma treated solution-processed nickel oxide: New insights into correlation of chemical and electronical properties, yet unpublished 2017.
31. P. A. Thiel and T. E. Madey, "The interaction of water with solid surfaces: Fundamental aspects," *Surf Sci Rep*, **7**, 211 (1987).
32. M. Motzko, M. A. Carrillo Solano, W. Jaegermann, and R. Hausbrand, "Photoemission Study on the Interaction Between LiCoO2 Thin Films and Adsorbed Water," *The Journal of Physical Chemistry C*, **119**, 23407 (2015).
33. W. Jaegermann and T. Mayer, "What do we learn from model experiments of semiconductor/electrolyte interfaces in UHV: coadsorption of Br2 with Na and H_2O on WSe2 (0001)," *Surf Sci*, **335**, 343 (1995).
34. W. Jaegermann and D. Schmeisser, "Simulation of photoactive semiconductor/electrolyte interfaces in the ultrahigh vacuum by adsorption of H2O and halogens on layered semiconductors, *AVS*, 1987.
35. T. Mayer and W. Jaegermann, "A Photoemission Study of Solute-Solvent Interaction: Coadsorption of Na and H∼ 2O on WSe∼ 2 (0001)," *J Phys Chem B*, **104**, 5945 (2000).
36. T. E. Madey and F. P. Netzer, "The adsorption of H2O on Ni (111); influence of preadsorbed oxygen on azimuthal ordering," *Surf Sci*, **117**, 549 (1982).
37. J. C. de Jesús, J. Carrazza, P. Pereira, and F. Zaera, "Hydroxylation of NiO films: the effect of water and ion bombardment during the oxidation of nickel foils with O2 under vacuum," *Surf Sci*, **397**, 34 (1998).
38. R. Furstenau, G. McDougall, and M. Langell, "Initial stages of hydrogen reduction of NiO (100)," *Surf Sci*, **150**, 55 (1985).
39. I. Saric, R. Peter, I. Kavre, I. J. Badovinac, and M. Petravic, "Oxidation of nickel surfaces by low energy ion bombardment," *Nuclear Instruments and Methods in Physics Research Section B: Beam Interactions with Materials and Atoms*, **371**, 286 (2016).
40. B. Payne, M. Biesinger, and N. McIntyre, "The study of polycrystalline nickel metal oxidation by water vapour," *J Electron Spectrosc*, **175**, 55 (2009).
41. R. L. Kurtz and V. E. Henrich, "Chemisorption of H_2O on the surface of Ti_2O3: Role of d electrons and ligand geometry," *Phys Rev B*, **26**, 6682 (1982).
42. T. Mayer, Photoelektronenspektroskopie an Modellgrenzflächen energiewandelnder Halbleiter: Adsorption, Koadsorption und Triadsorption von Br2, Na und H2O auf Van-der-Waals-Oberflächen von halbleitenden Metallchalkogeniden, *Universität Berlin*, 1993.
43. J. Dawson, Y. Guo, and J. Robertson, "Energetics of intrinsic defects in NiO and the consequences for its resistive random access memory performance," *Appl Phys Lett*, **107**, 122110 (2015).
44. A. Braun, Y. Hu, F. Boudoire, D. K. Bora, D. D. Sarma, M. Grätzel, and C. M. Eggleston, "The electronic, chemical and electrocatalytic processes and intermediates on iron oxide surfaces during photoelectrochemical water splitting," *Catalysis Today*, **260**, 72 (2016).
45. S. Tengeler, W. Calvet, M. Fingerle, C. Steinert, B. Kaiser, T. Mayer, and W. Jaegermann, "The impact of different Si surface terminations in the (001) n-Si/NiOx heterojunction on the oxygen evolution reaction (OER) by XPS and electrochemical methods, submitted to" *J. Electrochem. Soc.*, DOI (2017).
46. L. Trotochaud, J. K. Ranney, K. N. Williams, and S. W. Boettcher, "Solution-cast metal oxide thin film electrocatalysts for oxygen evolution," *J Am Chem Soc*, **134**, 17253 (2012).
47. K. M. Young and T. W. Hamann, "Enhanced photocatalytic water oxidation efficiency with Ni (OH) 2 catalysts deposited on α-Fe 2 O 3 via ALD," *Chem Commun*, **50**, 8727 (2014).
48. M. E. Lyons and M. P. Brandon, "The oxygen evolution reaction on passive oxide covered transition metal electrodes in aqueous alkaline solution. Part 1-Nickel," *Int. J. Electrochem. Sci*, **3**, 1386 (2008).
49. M. Wehrens-Dijksma and P. Notten, "Electrochemical Quartz Microbalance characterization of Ni (OH) 2-based thin film electrodes," *Electrochimica Acta*, **51**, 3609 (2006).